

Article

Power-Generation Optimization Based on Piezoelectric Ceramic Deformation for Energy Harvesting Application with Renewable Energy

Hyeonsu Han  and Junhyuk Ko *

Laboratory of Advanced Multi-Scale Manufacturing, Department of Mechanical Engineering, Korea Maritime and Ocean University, Busan 49112, Korea; gustn0211bye@g.kmou.ac.kr

* Correspondence: jko@kmou.ac.kr; Tel.: +82-514104292

Abstract: Along with the increase in renewable energy, research on energy harvesting combined with piezoelectric energy is being conducted. However, it is difficult to predict the power generation of combined harvesting because there is no data on the power generation by a single piezoelectric material. Before predicting the corresponding power generation and efficiency, it is necessary to quantify the power generation by a single piezoelectric material alone. In this study, the generated power is measured based on three parameters (size of the piezoelectric ceramic, depth of compression, and speed of compression) that contribute to the deformation of a single PZT (Lead zirconate titanate)-based piezoelectric element. The generated power was analyzed by comparing with the corresponding parameters. The analysis results are as follows: (i) considering the difference between the size of the piezoelectric ceramic and the generated power, 20 mm was the most efficient piezoelectric ceramic size, (ii) considering the case of piezoelectric ceramics sized 14 mm, the generated power continued to increase with the increase in the compression depth of the piezoelectric ceramic, and (iii) For piezoelectric ceramics of all diameters, the longer the depth of deformation, the shorter the frequency, and depending on the depth of deformation, there is a specific frequency at which the charging power is maximum. Based on the findings of this study, PZT-based elements can be applied to cases that receive indirect force, including vibration energy and wave energy. In addition, the power generation of a PZT-based element can be predicted, and efficient conditions can be set for maximum power generation.

Keywords: renewable energy; energy harvesting; piezoelectric ceramic; PZT; power generation



Citation: Han, H.; Ko, J.

Power-Generation Optimization Based on Piezoelectric Ceramic Deformation for Energy Harvesting Application with Renewable Energy. *Energies* **2021**, *14*, 2171. <https://doi.org/10.3390/en14082171>

Academic Editor: Dong-Wook Seo

Received: 18 March 2021

Accepted: 9 April 2021

Published: 13 April 2021

Publisher's Note: MDPI stays neutral with regard to jurisdictional claims in published maps and institutional affiliations.



Copyright: © 2021 by the authors. Licensee MDPI, Basel, Switzerland. This article is an open access article distributed under the terms and conditions of the Creative Commons Attribution (CC BY) license (<https://creativecommons.org/licenses/by/4.0/>).

1. Introduction

Renewable energy refers to the energy collected from resources such as the sun and ocean, which is naturally replenished over time and provides energy mainly for applications such as electricity generation and heat production [1,2]. Of late, due to concerns regarding environmental issues such as climate change and global warming, research on renewable energy harvesting systems is being actively pursued along with the increase in renewable energy development.

Among these renewable energies, wave power generation is an ocean energy that primarily utilizes the vibration energy of waves. As wave power generation has relatively lower regional restrictions than power generation based on seawater temperature difference or tidal streams, it has high potential for development [3,4]. Moreover, its power density is 10 times higher than that of the other renewable energies and it can be easily predicted based on the weather forecast; hence, energy harvesting is easy. However, mooring wave power plants in the ocean for large-scale energy harvesting is economically disadvantageous because they are vulnerable to corrosion, and the associated installation cost increases [5,6]. In this study, a piezoelectric energy harvesting system is used to improve the efficiency of

wave energy and vibration energy, which are difficult to develop due to concerns such as economic problems.

Energy harvesting is a technology that converts the energies generated from external sources such as renewable energy into electrical energy. There are various types of energy harvesting systems, including light energy, gravitational energy, and body energy. Recently, the piezoelectric energy harvesting system has been extensively applied in various fields because it is inexpensive [7–10].

Piezoelectric energy is the energy collected in a solid substance such as ceramic or crystal in response to latent heat or mechanical stress. It features a lightweight, compact, and a rapid and simple conversion mechanism [11–14]. As piezoelectric energy is aimed at charging low-power storage devices such as batteries and capacitors, it assists in harvesting useful energy, reducing the production and maintenance costs of energy with low production efficiency, and reducing the chemical waste energy from battery replacement. Therefore, piezoelectric energy is applied in several industries such as manufacturing and automobiles [15–18].

As an application example of piezoelectric energy harvesting, Sun et al. utilized the piezoelectric equation to increase the efficiency of the low-frequency energy harvesting existing in the surrounding area [19]. They studied a theoretical model stacked in serial or parallel in the d_{33} mode [20,21], in which stress is applied in the axial direction of the front part of the piezoelectric ceramic [22,23]. Truitt et al. modeled a PVDF (Polyvinylidene fluoride) piezoelectric flag system and proposed an approach for wind-based piezoelectric energy harvesting [24]. Fang et al. studied a vibration energy recovery system through the structure of a piezoelectric composite cantilever generator [25]. Viet et al. investigated a floating energy harvester for harvesting wave energy using the piezoelectric effect [26–29]. Further, they harvested energy in intermediate and deep waters [30]. Moreover, Li et al. developed an ocean wave energy harvester using the piezoelectric effect from the transverse wave motion of water particles [31].

The above studies strive to combine piezoelectric energy and renewable energy such as the vibration energy of the wind or waves in an energy harvesting system. However, it is necessary to quantify the power generated by the deformation of the piezoelectric before calculating the power efficiency of piezoelectric energy combined with various renewable energies.

This study measured the voltage/current generated by stress in a specific PZT-based piezoelectric ceramic [32,33] of a circular diaphragm transducer, and confirmed the relationship between the power generated and the deformation of the piezoelectric ceramic. To understand this relationship, experiments were performed 10 times by specifying three parameters that contributed to the deformation, and their average was considered as the experimental result. Furthermore, the experimental results were used to analyze the comparative relationships among the parameters after converting the measured charging voltage and current to power. By analyzing the relationships among the parameters that contribute to the deformation of the piezoelectric ceramic and the power generated, it is possible to predict the power generated by a specific piezoelectric ceramic in combination with various renewable energies related to vibration energy. This can be applied for predicting the relatively high-efficiency power generation from the fine energy generated within port structures or ships.

The sequence of this study consists of experimental contents including data collection method and parameters, starting with the material description of a single piezoelectric element (PZT). Section 4 shows the results of charging power for three parameters, and Section 5 concludes.

2. Materials

2.1. Piezoelectric Material

In this study, we used five PZT-based elements. The five types of elements were divided into ceramic PZT diameters, which were divided into 11 mm, 14 mm, 20 mm,

25 mm, and 50 mm, respectively, and the ceramic thickness was the same as 0.2 mm. A model of a PZT-based elements is shown in Figure 1, which is a piezoelectric transducer structure with a circular diaphragm. As shown in Figure 1, the circular diaphragm structure was divided into a circular metal sheet (copper) and a piezoelectric ceramic layer, and it was composed of two electrode layers attached above and below the piezoelectric ceramic layer.

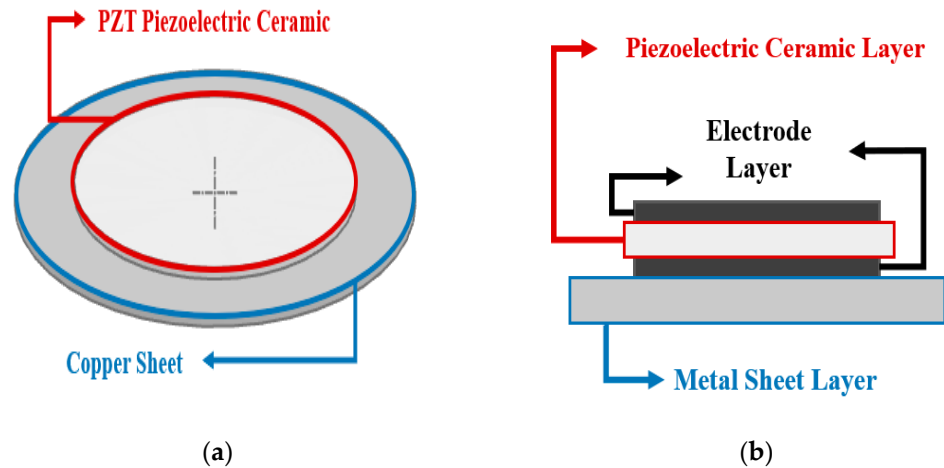


Figure 1. PZT based element: (a) front view; (b) side view.

PZT (Lead Zirconate Titanate; $Pb [Zr (x) Ti (1 - x)] O_3$), which constitutes the piezoelectric ceramic layer, is a lead-based material as a type of piezoelectric material. It has the advantages of high piezoelectric effect, low dielectric loss, and compatibility with MEMS (Micro Electro Mechanical Systems) production. Although it has been replaced by lead-free materials such as $BaTiO_3$ due to lead toxicity, it is still most used in piezoelectric generators. PZT is a polycrystalline material with a perovskite crystal structure and is shown in Figure 2.

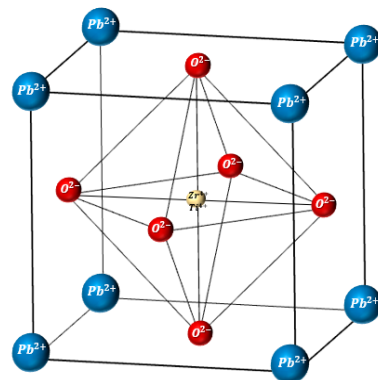


Figure 2. Perovskite crystal structure.

2.2. Piezoelectric Effect

When the piezoelectric material is viewed in crystal lattice structure units, the positions of positive and negative charges are slightly different, and an electric field is formed around the atoms or molecules, which is an electric dipole. PZT is one of the materials of the electric dipole. When the stress or electric field of these materials is applied, the positions between the atoms or molecules that comprise the crystal change. Hence, polarization occurs that creates a dipole moment. In the process of polarization generation, the piezoelectric material becomes piezoelectricity. Piezoelectricity means “charges generated by stress applied to materials with structures such as perovskite crystals” or “electrical behavior of ceramics and crystals belonging to a mechanical structure and a particular assessment”. The piezoelectric effect indicates these piezoelectricity phenomena. The piezoelectric effect is

divided into two phenomena. There is a direct piezoelectric effect that generates an electric field when a stress is applied to the piezoelectric material and a converse piezoelectric effect that deforms the piezoelectric material when an electric field is applied.

In this study, we used the direct piezoelectric effect that generates an electric field when a stress is applied to a PZT-based element, which is represented in Figure 3.

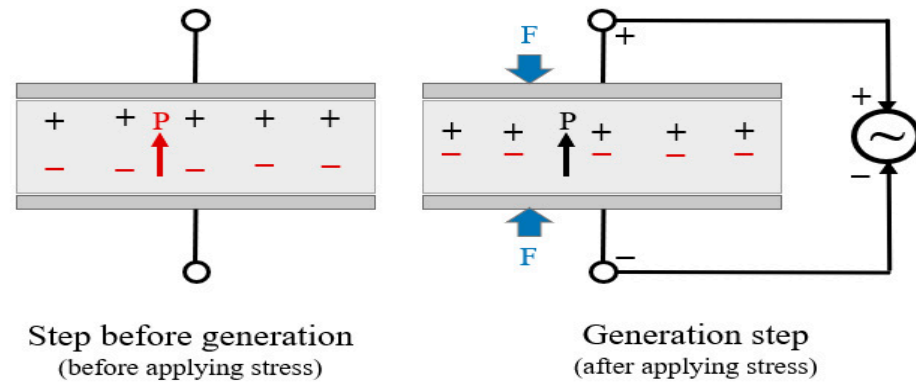


Figure 3. Illustration of the direct piezoelectric effect.

2.3. d_{33} Mode (Piezoelectric Transverse Mode)

PZT-based elements generate an electric field when contraction or expansion occurs between the electrode layers. At this time, an actuation force is produced in the piezoelectric ceramic layer, and the stress direction and the electric field indicate the working modes as shown in Figure 4. Figure 4a shows the d_{33} mode in which the applied stress and the generated electric field are the same in the transverse direction (3 direction). It is mainly used for the stack-type transducer. On the other hand, Figure 4b shows the d_{31} mode, and the applied stress is the Longitudinal direction (1 direction), a generated electric field is the transverse direction (3 direction). It has been extensively studied using cymbal or cantilever type transducers.

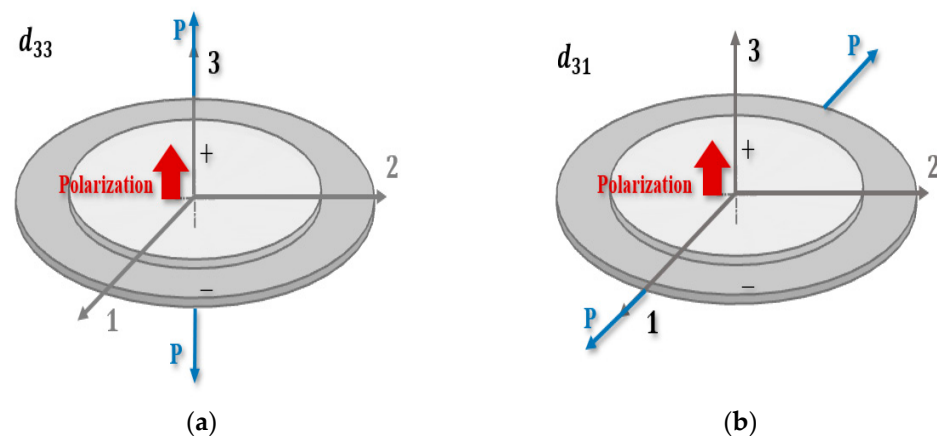


Figure 4. Working mode: (a) Transverse mode (d_{33} mode); (b) Longitudinal mode (d_{31} mode).

In this study, we used the d_{33} mode, which applied stress in the transverse direction (3 direction) to a PZT-based element of a circular diaphragm type piezoelectric transducer and generated the electric field in the same direction (transverse direction/3 direction).

3. Experimental

This experiment used five PZT-based elements of a circular diaphragm piezoelectric transducer. The used five PZT-based elements were piezoelectric ceramic PZT with diameters of 11 mm, 14 mm, 20 mm, 25 mm, and 50 mm, respectively (SMG Catalog number 1361121,

1361186, 1361133, 1361122, and GO'SUN Catalog number 4903791962, respectively). And the thickness of all piezoelectric ceramics was equal to 0.2 mm. The experiment was set to measure the voltage and current generated through a piezoelectric charging circuit with continuous stress in the plunger, shown in Figure 5. As shown in Figure 5, the PZT-based element connected to the piezoelectric charging circuit and is supported by a TPU(Thermoplastic Polyurethane)-made case. A flexible form of TPU material was used so as not to interfere with the deformation that occurs when stress is applied to the piezoelectric element using the plunger. Moreover, the electric wire connected to the metal sheet was allowed to pass through the TPU-made case, and the design is as shown in Figure 6.

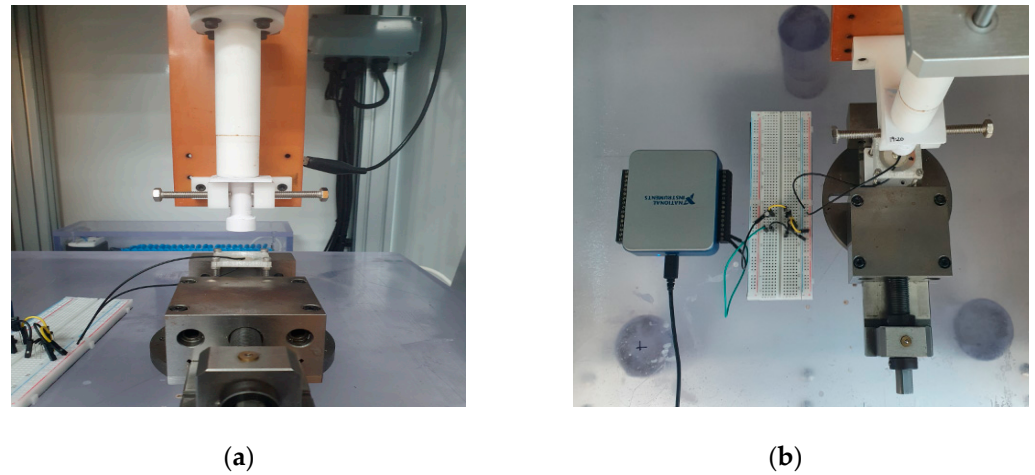


Figure 5. Experimental setup: (a) Front view; (b) Top view.

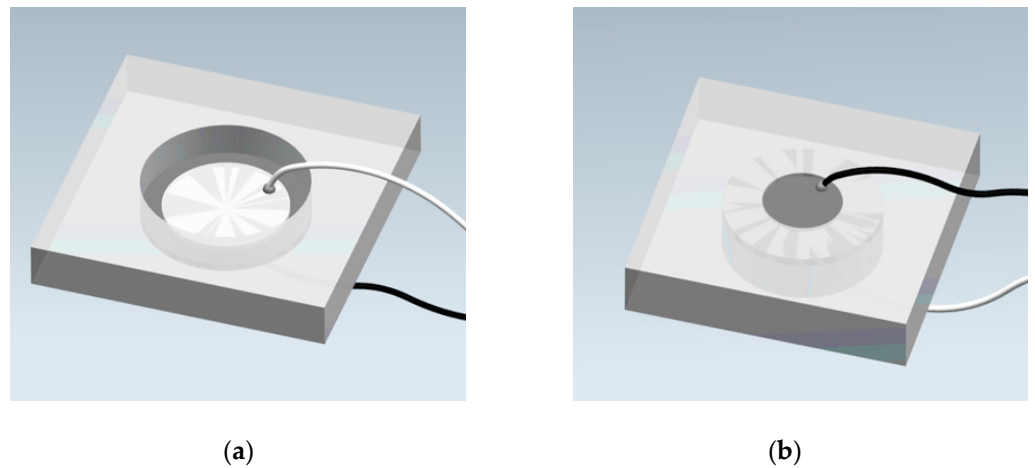


Figure 6. TPU-made case model: (a) Top view; (b) Bottom view.

The reason why the piezoelectric element was not fixed from the side is to prevent deformation of bending or breaking that occurs when more than a certain amount of stress is applied. The piezoelectric charging circuit was designed for the bridge diode rectification circuit shown in Figure 7. Three parameters that contributed to the deformation of the piezoelectric element were selected as the experimental parameters and indexed for convenient comparison, as shown in Table 1. The charging voltage and current were measured using LabVIEW software and a DAQ board (DAQ USB-6003); five data were collected per second.

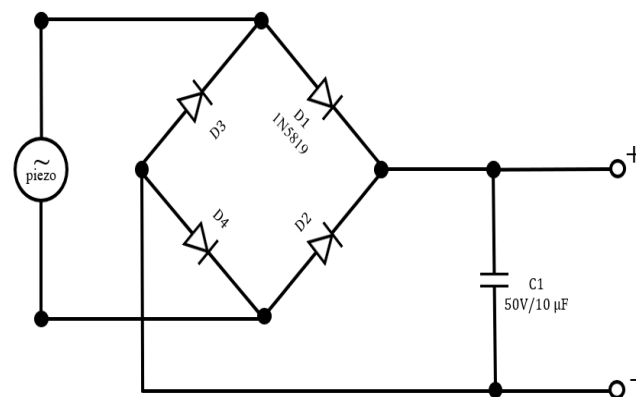


Figure 7. Bridge diode rectification circuit (piezoelectric charging circuit).

Table 1. Parameter index.

Parameter	Index
x mm Diameter of the piezoelectric ceramic (PZT)	S_x
x mm Deformation Depth of the piezoelectric ceramic (PZT)	D_x
x Hz Deformation Frequency of the piezoelectric ceramic (PZT)	f_x

3.1. Data Collection Method

The unit of the voltage generated when stress is applied to a piezoelectric element is mV and the unit of the current is μA . As the measured current when is applied one period stress is very small, there is a possibility that the accuracy may be degraded by measurement noise. Hence, one experiment was conducted by fixing the applied stress period to 10 times. the experiment was conducted by fixing the number of stress cycles to 10. In addition, considering the error in the diameter of the piezoelectric ceramic (S_x) attached to the PZT-based element, the result data for each parameter was derived by averaging the values of 10 experiments.

3.2. Parameter

The first parameter was the diameter of the piezoelectric ceramic (S_x), which indicated the diameter of the piezoelectric ceramic attached to the front surface of the metal sheet(copper). Four PZT-based elements for each diameter were selected from products of the same manufacturer: 11 mm(S_{11}), 14 mm(S_{14}), 20 mm(S_{20}) and 24 mm(S_{24}). We selected a PZT-based device from another manufacturer: 50 mm(S_{50}). This was included in the parameter because it had the same piezo ceramic thickness (0.2 mm) and metal sheet (copper) as the previous PZT-based elements, but the piezo ceramic diameter was so large.

The second parameter is the deformation depth of the piezoelectric ceramic (D_x) is compressed by the applied stress. It indicates the depth compressed downward at the zero points, which are the points that contact the front of the piezoelectric element and the plunger. Three depth parameters were selected for comparing piezoelectric elements of all diameters: 1 mm(D_1), 2 mm(D_2) and 3 mm(D_3). When stress is applied to piezoelectric ceramics with diameters of S_{11} and S_{14} to a depth of D_3 or more, the piezoelectric ceramic broke or the copper sheet was bent. When such phenomena occur, breakage takes place immediately and the charging value decreases, or charging is not possible. Figure 8 shows different charging curves depending on when the piezoelectric device is partially damaged and when it is completely damaged.

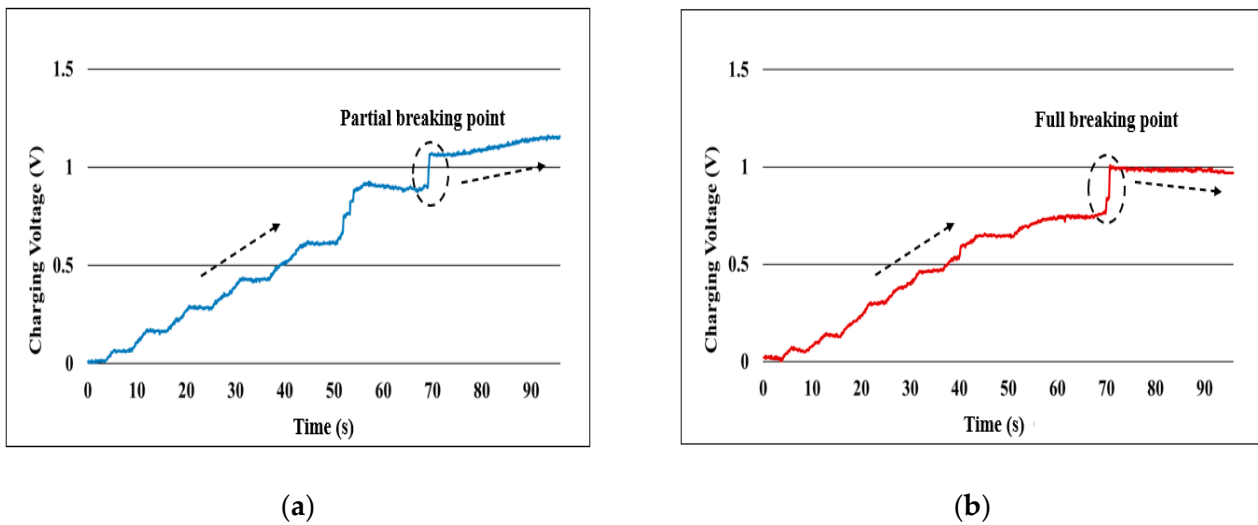


Figure 8. Breaking point: (a) partial; (b) full.

The third parameter is the input frequency of the plunger (f_x). The input frequency is that it moves several cycles per second. The input frequency changes depending on the deformation depth of the piezoelectric ceramic and the speed of the plunger. Depending on the deformation depth of the piezoelectric ceramic, the length of the cycle changes, and the distance compressed for 1 second changes depending on the speed of the plunger. The speed of the plunger used in this experiment can be set at 1 mm/s min intervals from 1 mm/s to 16 mm/s max. The cycle length is 2 mm, 4 mm and 6 mm depending on the depth of deformation (1 mm, 2 mm and 3 mm). A comparable frequency interval was specified at 1 Hz in response to a 1 mm/s speed change, and a total of four parameters were selected: 1 Hz(f_1), 2 Hz(f_2), 3 Hz(f_3) and 4 Hz(f_4). when the cycle length is 6 mm, the frequencies of 3 Hz and 4 Hz were excluded because the plunger speeds of 18 mm/s and 24 mm/s could not be set.

The expression of the three type parameters (diameter of the piezoelectric ceramic (S_x), deformation depth of the piezoelectric ceramic (D_x), and input Frequency of the plunger (f_x) is shown in Figure 9.

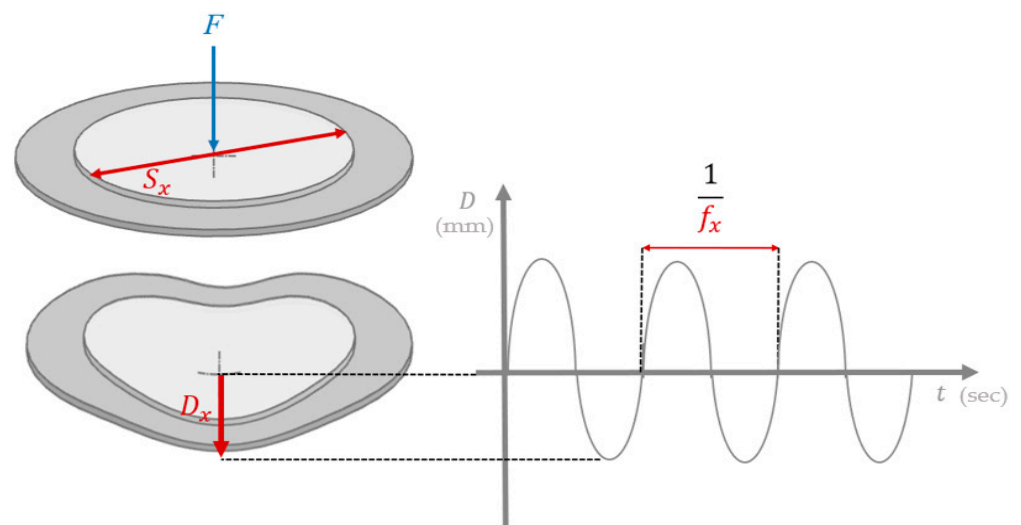


Figure 9. Schematic of parameters deformation.

4. Results for the Charging Power

We measured the voltage and current using the DAQ (Data Acquisition) board USB-6003 and LabVIEW software (Korea National Instruments Co., Ltd. Seoul, Korea). Further, the charging power was calculated as the product of the measured voltage and current as per Equation (1) and compared.

$$P(W) = V(V) \times I(A) \quad (1)$$

4.1. Diameter of The Piezoelectric Ceramic (S_x)

After fixing the second parameter (D_x) and the third parameter (f_x), the charge values of the diameter of each piezoelectric ceramic (S_x) were compared. Figure 10, Figure 11, and Figure 12 are all graphs comparing S_x , and each figure number is divided into D_x for easy comparison on the y-axis. The x-axis piezoelectric ceramic diameter (S_x) of each graph, and the y-axis is the charging power (P).

Charging power increases for all S_x values. The comparison of S_x values was analyzed by the ratio of the difference in charging power of both S_x . The ratio of charging power of S_{14} and S_{20} was 2:8 on average. However, the ratio of charging power between S_{20} and S_{24} was about 4:6. Considering these ratios, when S_x increased, the charging power increases, but the piezoelectric ceramic that had a high-power generation amount compared to the size is S_{20} .

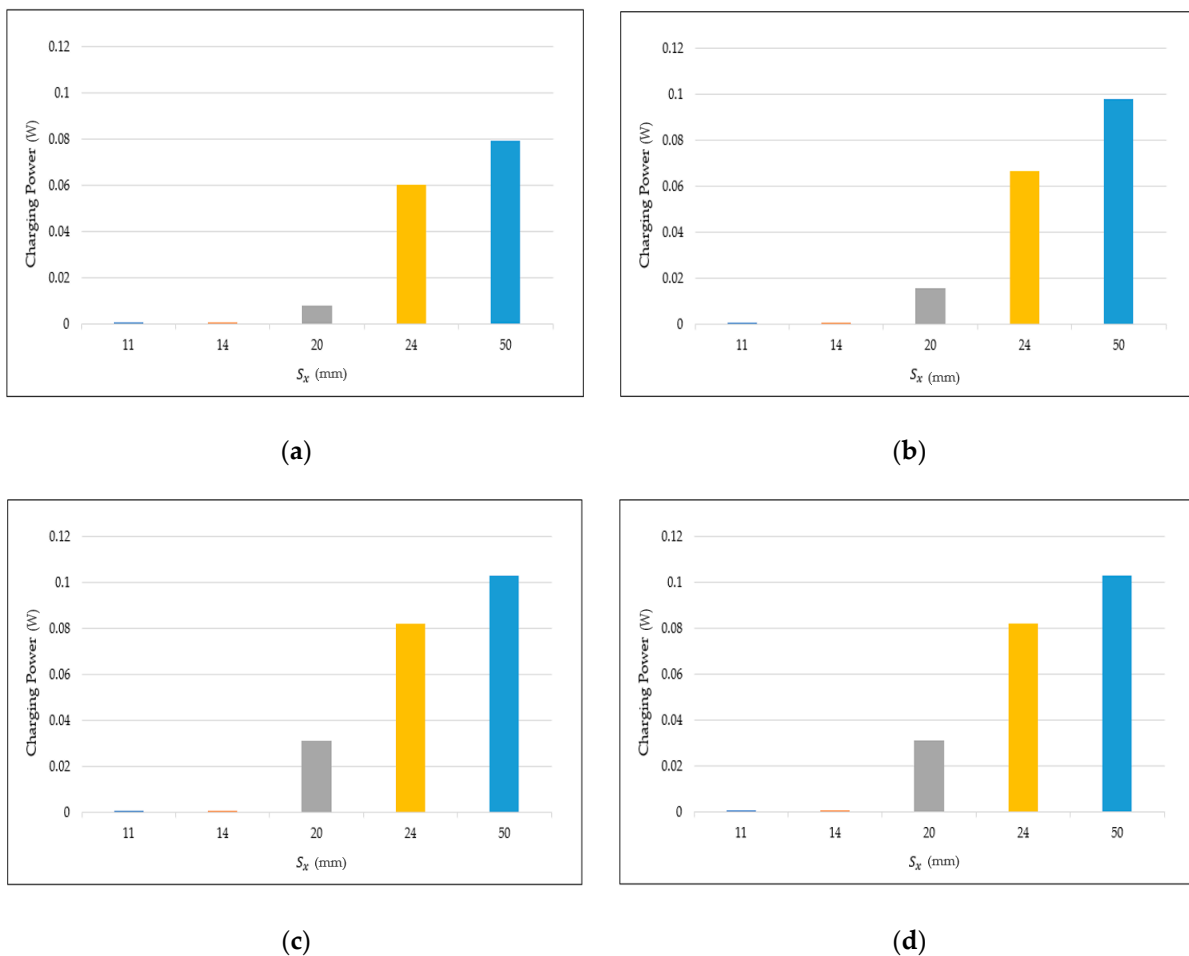


Figure 10. Comparison of the charging power according to S_x for D_1 : (a) f_1 ; (b) f_2 ; (c) f_3 ; (d) f_4 .

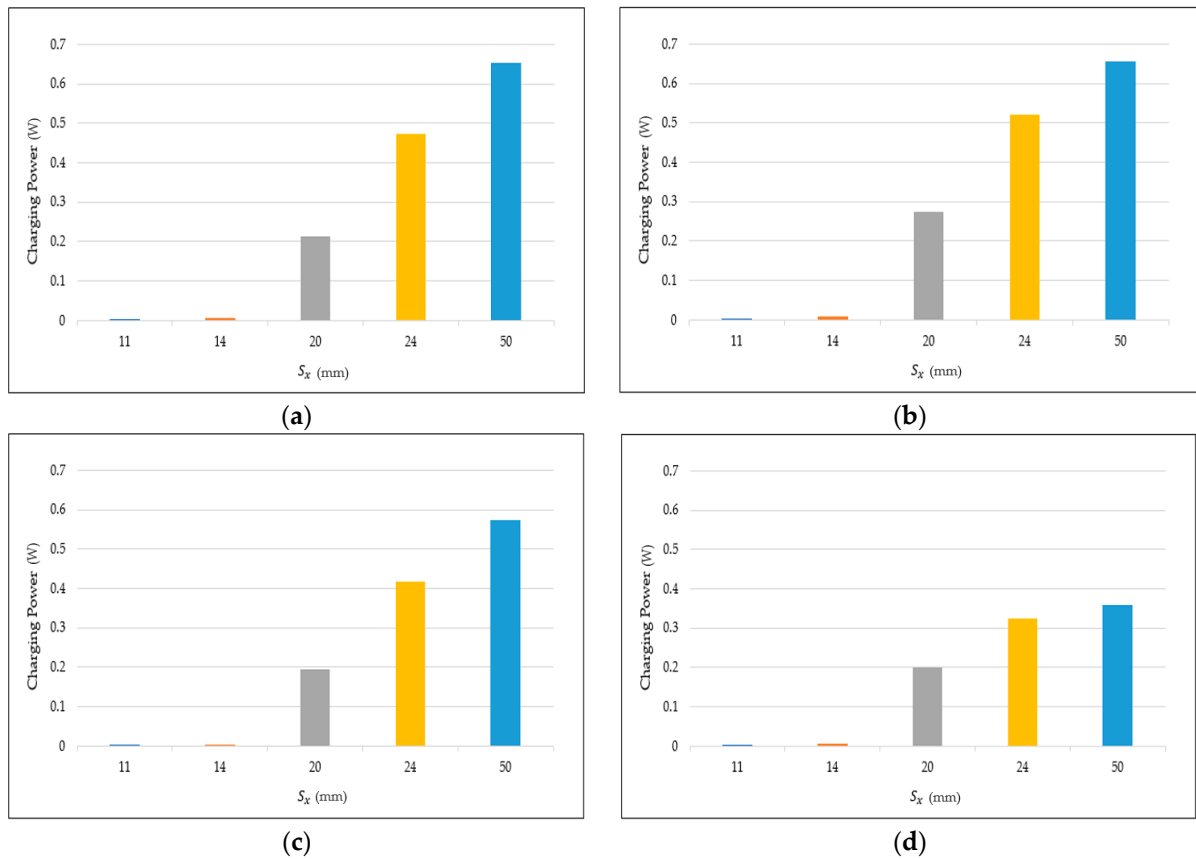


Figure 11. Comparison of the charging power according to S_x for D_2 : (a) f_1 ; (b) f_2 ; (c) f_3 ; (d) f_4 .

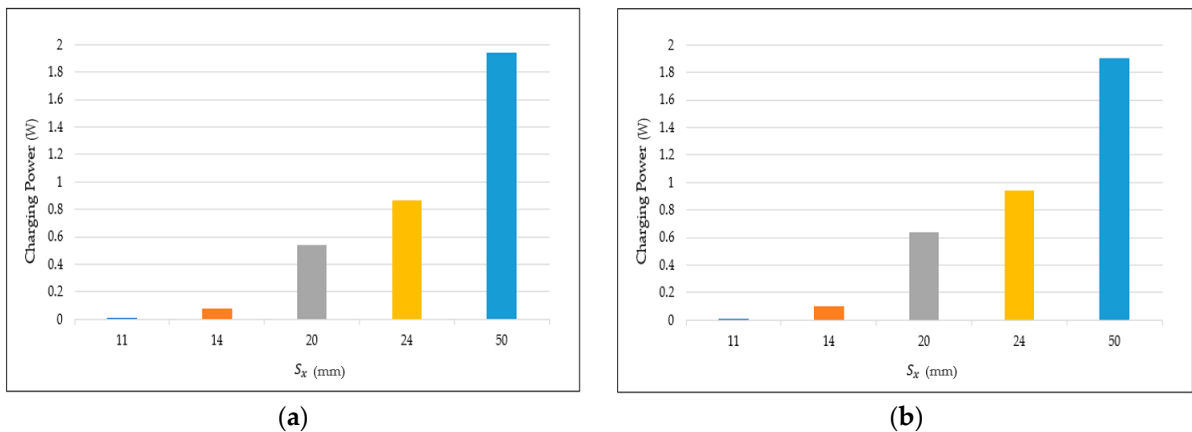


Figure 12. Comparison of the charging power according to S_x for D_3 : (a) f_1 ; (b) f_2 .

4.2. Depth to Which the Piezoelectric Ceramic is Compressed (D_x)

After fixing the first parameter (S_x) and the third parameter (f_x), the charge values of the deformation depth of each piezoelectric ceramic (D_x) were compared. Figures 13–17 are all graphs comparing D_x , and each figure number is divided into S_x for easy comparison on the y-axis. The x-axis deformation depth (D_x) of each graph, and the y-axis is the charging power (P). Data were collected by applying stress to the maximum depth to the breaking point to compare all parameters. At D_3 and above, breaking points easily occur at S_{11} and S_{14} . Therefore, a stress of D_3 or higher was applied to analyze the charging power of all D_x .

Charging power for all D_x values increased. As the charging voltage of S_{11} and S_{14} continued to increase, the voltage generated when the piezoelectric ceramic along with

the other S_x was compressed to a larger D_x can increase. However, it was judged that the larger the value of D_x , the longer the period during which stress was applied, and the farther the form was from the wave energy and vibration energy considered in this study.

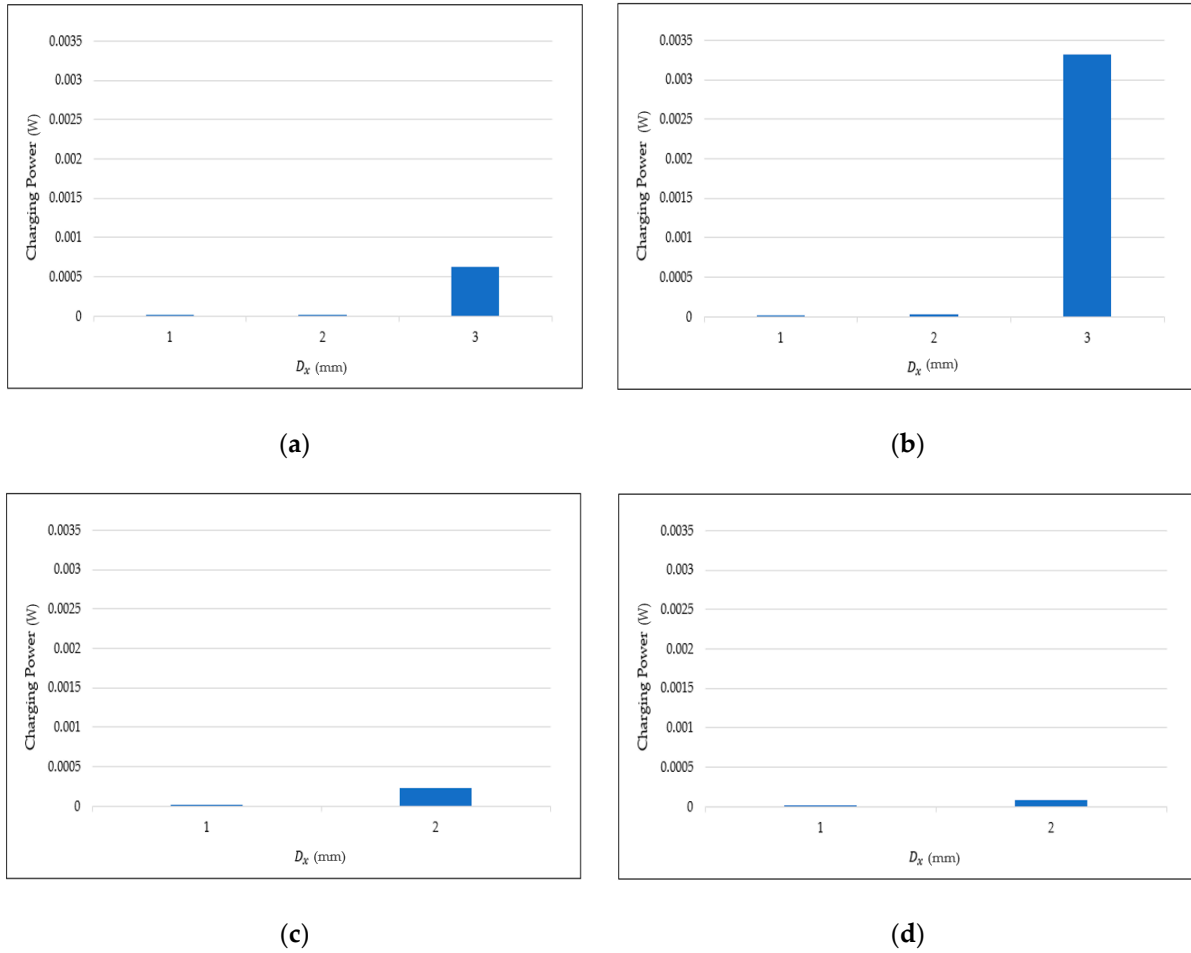


Figure 13. Comparison of the charging power according to D_x for S_{11} : (a) f_1 ; (b) f_2 ; (c) f_3 ; (d) f_4 .

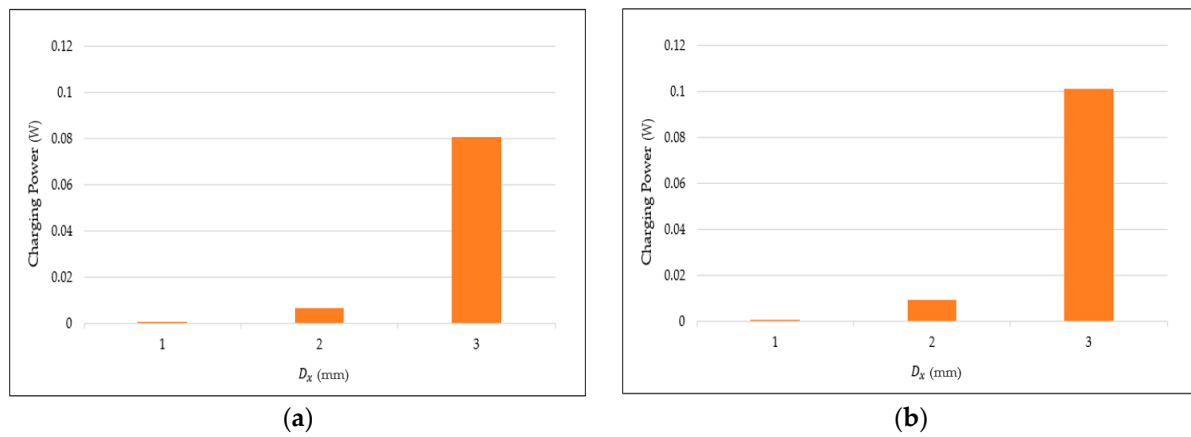


Figure 14. Cont.

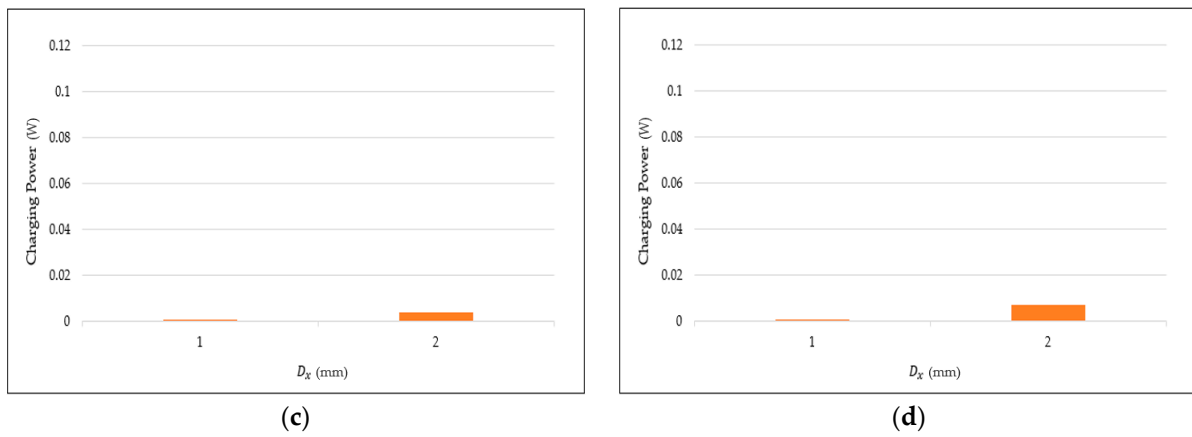


Figure 14. Comparison of the charging power according to D_x for S_{14} : (a) f_1 ; (b) f_2 ; (c) f_3 ; (d) f_4 .

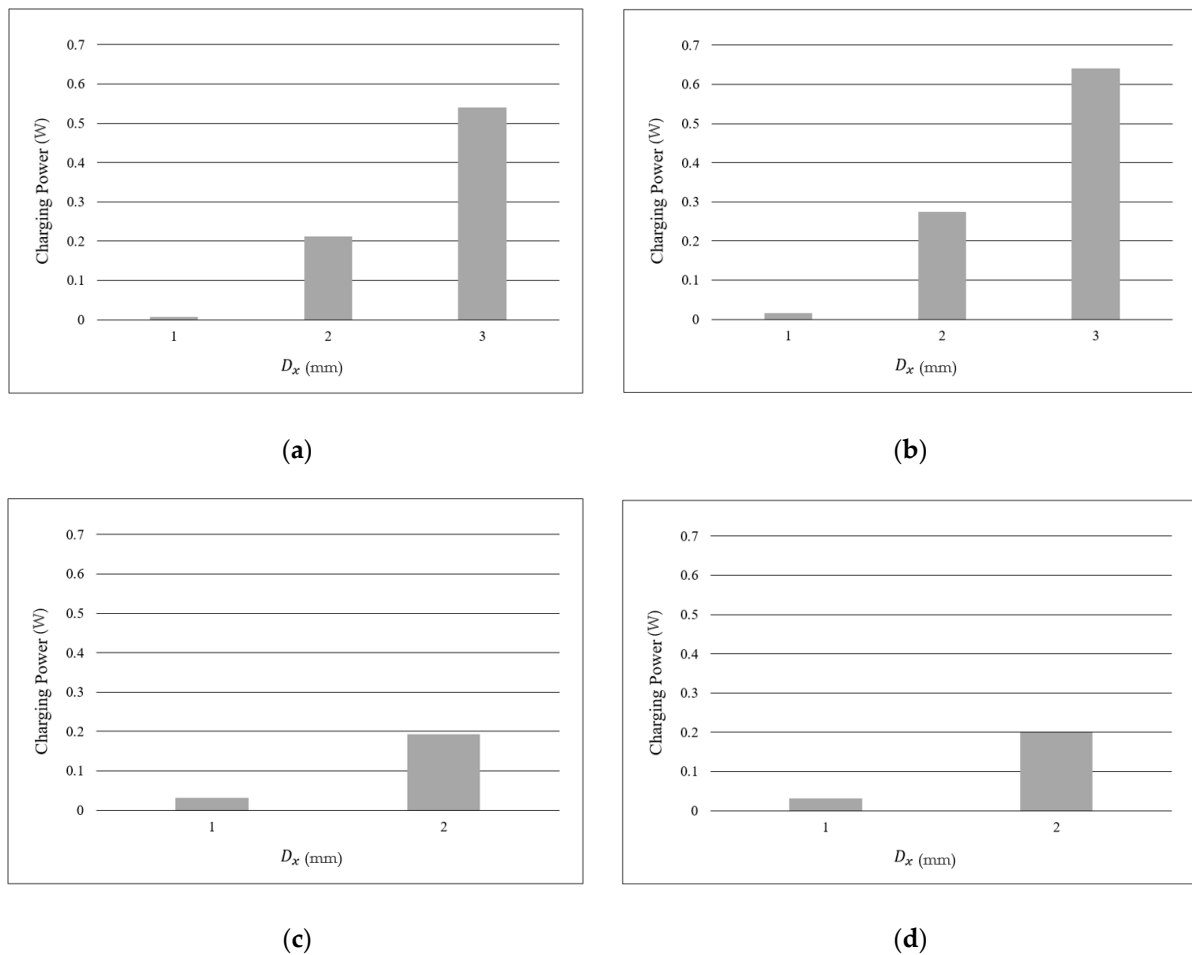


Figure 15. Comparison of the charging power according to D_x for S_{20} : (a) f_1 ; (b) f_2 ; (c) f_3 ; (d) f_4 .

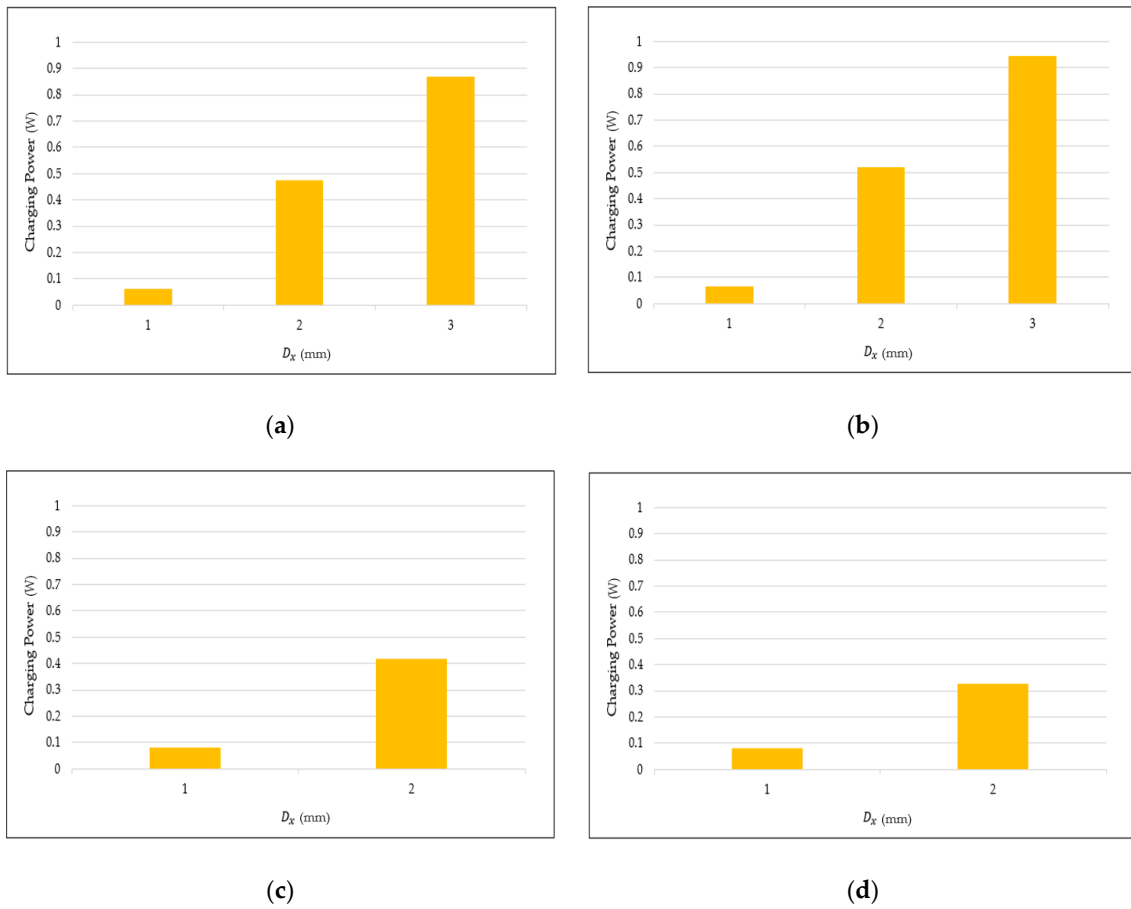


Figure 16. Comparison of the charging power according to D_x for S_{24} : (a) f_1 ; (b) f_2 ; (c) f_3 ; (d) f_4 .

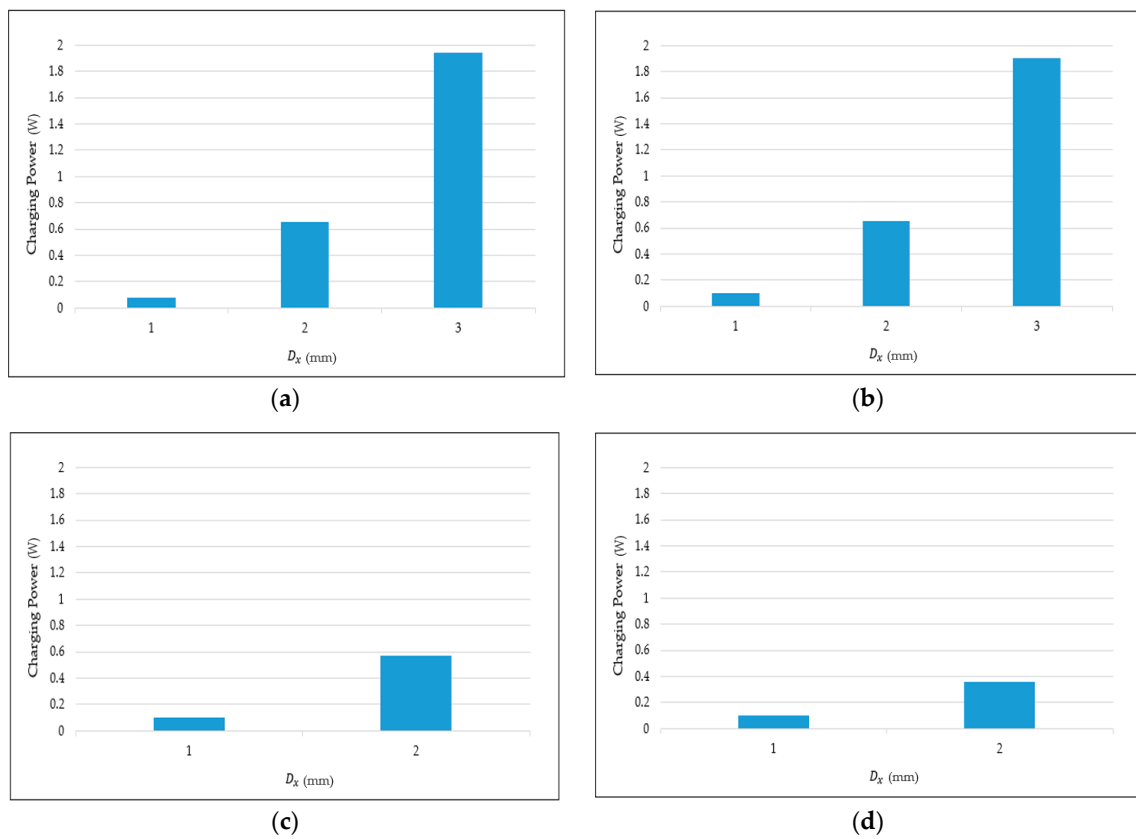
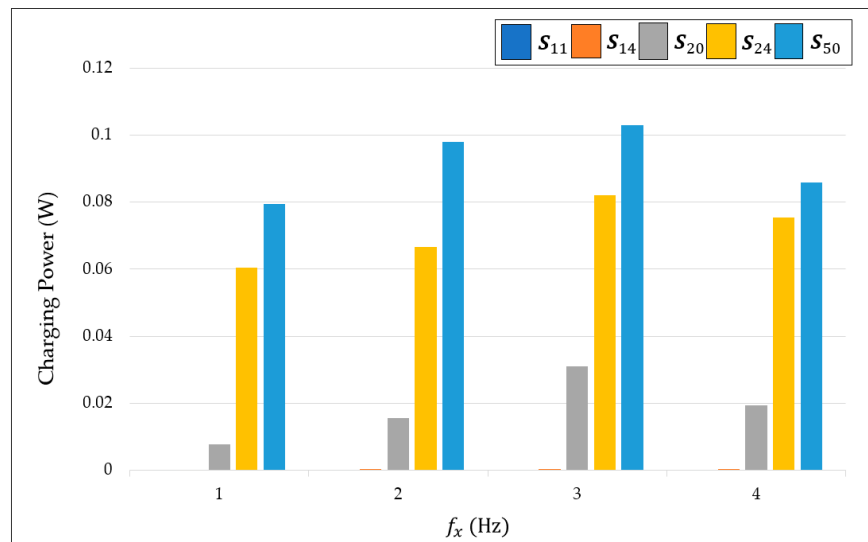


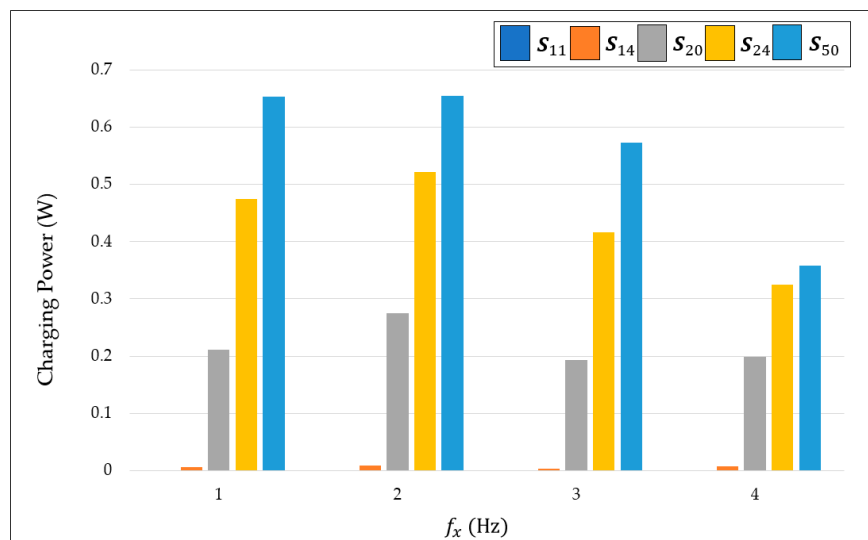
Figure 17. Comparison of the charging power according to D_x for S_{50} : (a) f_1 ; (b) f_2 ; (c) f_3 ; (d) f_4 .

4.3. Input Frequency of the Plunger (f_x)

After fixing the first parameter (S_x) and the second parameter (D_x), the charge values of the input frequency of the plunger (f_x) were compared. Figure 18 is a graph comparing f_x . The x-axis input frequency (f_x) of each graph, and the y-axis is the charging power (P). The reason why f_3 and f_4 are not present in Figure 18c is that the corresponding speeds (18 mm/s, 24 mm/s) of the plunger cannot be set. Therefore, Figure 18c is difficult to analyze. Also, for S_{11} and S_{14} , a charging power value of less than 0.001W (1mW) is incorrect due to noise if the ceramic is damaged.



(a)



(b)

Figure 18. Cont.

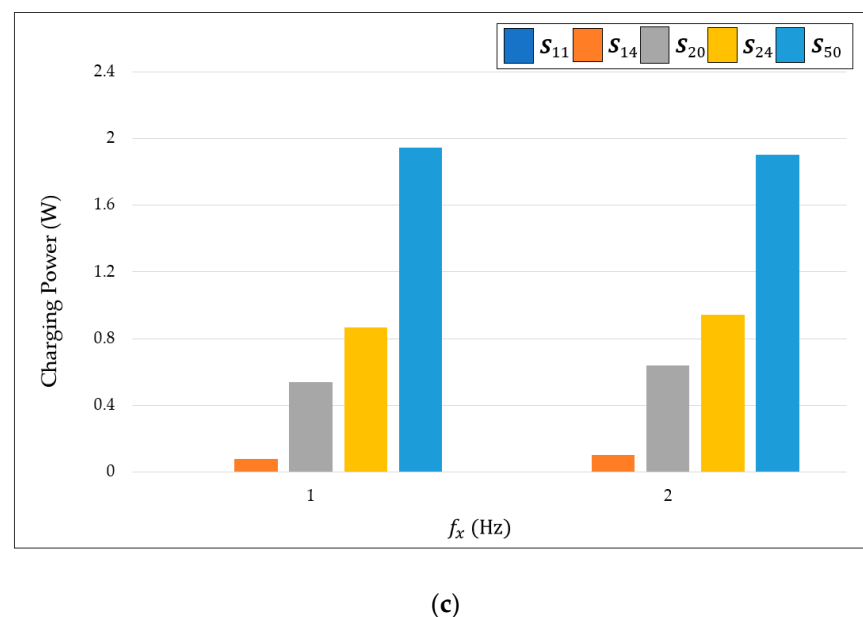


Figure 18. Comparison of the charging power according to f_x : (a) D_1 ; (b) D_2 ; (c) D_3 .

The input frequency of the plunger that maximized the charging power in Figure 18a was 3 Hz. In Figure 18b, the input frequency of the plunger that maximized the charging power was 2 Hz. This shows the same result for all S_x in each graph. Each graph represents D_1 and D_2 , and the frequency tends to become shorter as the depth of deformation increases. Based on the depth of deformation D_x from all S_x , we expect that there is a specific f_x with the maximum charging power.

5. Conclusions

Energy harvesting techniques such as piezoelectric energy generation can harvest useful energy from energy that has low production efficiency. Due to the low range of piezoelectric energy harvesting, it can be used for amplifying power generation in various applications. Piezoelectric elements can be connected in series or parallel to accumulate the generated power or can be combined with renewable energy to amplify power generation. However, as no data is available on the power generated by a single piezoelectric element, it is difficult to predict the amplified energy, unless an experiment is performed after amplifying the energy from a single piezoelectric.

In this study, the generated power by a specific piezoelectric element, namely a PZT-based piezoelectric ceramic, was measured. Focusing on the deformation that affects piezoelectric ceramic power generation, the results of piezoelectric power generation for three parameters that contribute to the deformation are as follows: (i) as the size of piezoelectric ceramic increases, the generated power increases, but the ratio is not proportional. Accordingly, considering the difference in the size of the piezoelectric ceramic and the power generated by each, S_{20} is the most efficient. (ii) The generated power continues to increase with the deformation depth of the piezoelectric ceramic up to the point where the piezoelectric ceramic or the piezoelectric element breaks. (iii) For piezoelectric ceramics of all diameters, the longer the depth of deformation, the shorter the frequency, and depending on the depth of deformation, there is a specific frequency at which the charging power is maximum. It is necessary to analyze the frequency corresponding to the deeper deformation depth. Based on the results of this study, PZT-based elements can be applied to cases that receive indirect force, including vibration energy and wave energy. In addition, the power generation of a PZT-based element can be predicted and efficient conditions can be set for maximum power generation. Following this study, the power generated by connecting several piezoelectric elements will be increased, and further studies will be conducted on the combination of wave and vibration energy.

Author Contributions: H.H. and J.K. contributed to the design and implementation of the research, to the analysis of the results, and to the writing of the manuscript. Both authors have read and agreed to the published version of the manuscript.

Funding: This research was supported by Basic Science Research Program through the National Research Foundation of Korea (NRF) funded by the Ministry of Education and Ministry of Science (2019R1G1A1009980).

Institutional Review Board Statement: Not applicable.

Informed Consent Statement: Not applicable.

Data Availability Statement: Not applicable.

Acknowledgments: The paper was supported by NRF, Korea, under Grant number(2019R1G1A1009980).

Conflicts of Interest: The authors declare no conflict of interest.

References

1. Ellabban, O.; Abu-Rub, H.; Blaabjerg, F. Renewable energy resources: Current status, future prospects and their enabling technology. *Renew. Sustain. Energy Rev.* **2014**, *39*, 748–764. [CrossRef]
2. Sawin, J.L.; Martinot, E. Renewables 2010-Global Status Report. REN21 Secretariat 2014. Available online: https://www.harbertaxgroup.com/wp-content/uploads/2014/07/REN21_GSR_2010_full_revised-Sept2010.pdf (accessed on 1 September 2010).
3. Callaghan, J.; Boud, R. Future Marine Energy: Results of the Marine Energy Challenge: Cost Competitiveness and Growth of Wave and Tidal Stream Energy. *Carbon Trust* **2006**, *40*. Available online: https://www.bchydro.com/content/dam/hydro/medialib/internet/documents/planning_regulatory/iep_itap/ror/appx_11a_marine_energy.pdf (accessed on 1 January 2006).
4. Czech, B.; Bauer, P. Wave energy converter concept: Design challenges and classification. *IEEE Ind. Electron. Mag.* **2012**, *6*, 4–16. [CrossRef]
5. Falnes, J. A review of wave-energy extraction. *Mar. Struct.* **2007**, *20*, 185–201. [CrossRef]
6. Smil, V. *Energy in Nature and Society: General Energetics of Complex Systems*; MIT Press: Cambridge, MA, USA, 2008.
7. Erturk, A.; Inman, B.J. *Piezoelectric Energy Harvesting*; John Wiley & Sons: Hoboken, NJ, USA, 2011.
8. Barbehenn, G.H. True grid independence: Robust energy harvesting system for wireless sensors uses piezoelectric energy harvesting power supply and li-poly batteries with shunt charger. *LT J. Analog Innov.* **2010**, *20*, 36–38.
9. Rjafallah, A.; Hajjaji, A.; Guyomar, D. Modeling of polyurethane/lead zirconate titanate composites for vibration energy harvesting. *J. Compos. Mater.* **2018**, *53*, 613–623. [CrossRef]
10. Gareh, S.; Kok, B.C.; Yee, M.H. Optimization of the Compression-Based Piezoelectric Traffic Model (CPTM) for Road Energy Harvesting Application. *Int. J. Renew. Energy Res.* **2019**, *9*, 1272–1282.
11. Ballato, A. Piezoelectricity: Old, new thrusts. *IEEE Trans. Ultrason. Ferroelectr. Freq. Control* **1995**, *42*, 916–926. [CrossRef]
12. Ballato, A. Piezoelectricity: History and new thrusts. *IEEE Ultrason. Symp. Proc.* **1996**, *1*, 575–783.
13. Luo, Z.; Zhu, D.; Beeby, S.P. Multilayer ferroelectret-based energy harvesting insole. *J. Phys. Conf. Ser.* **2015**, *660*, 012118. [CrossRef]
14. Kim, K.N.; Chun, J.; Chae, S.A. Silk fibroin-based biodegradable piezoelectric composite nanogenerators using lead-free ferroelectric nanoparticles. *Nano Energy* **2015**, *14*, 87–94. [CrossRef]
15. Platt, S.R.; Farritor, S.; Haider, H. On low-frequency electric power generation with PZT ceramics. *IEEE/ASME Trans. Mechatron.* **2005**, *10*, 240–252. [CrossRef]
16. Yan, X.; Li, G.; Wang, Z. Recent progress on piezoelectric materials for renewable energy conversion. *Nano Energy* **2020**. [CrossRef]
17. Chen, H.; Jia, C. Power harvesting with PZT ceramics. In Proceedings of the 2007 IEEE International Symposium on Circuits and Systems, New Orleans, LA, USA, 27–30 May 2007; pp. 557–560.
18. Liu, H.; Hua, R.; Lu, Y. Boosting the efficiency of a footstep piezoelectric-stack energy harvester using the synchronized switch technology. *J. Intell. Mater. Syst. Struct.* **2019**, *30*, 813–822. [CrossRef]
19. Sun, C.; Shang, G. Modeling for piezoelectric stacks in series and parallel. In Proceedings of the 2013 Third International Conference on Intelligent System Design and Engineering Applications, Hong Kong, China, 16–18 January 2013; pp. 954–957.
20. Khalid, S.; Raouf, I.; Khan, A. A Review of Human-Powered Energy Harvesting for Smart Electronics: Recent Progress and Challenges. *Int. J. Precis. Eng. Manuf. Green Technol.* **2019**, *6*, 821–851. [CrossRef]
21. Nguyen, C.H.; Hanke, U.; Halvorsen, E. Actuation of Piezoelectric Layered Beams With d₃₁ and d₃₃ Coupling. *IEEE Trans. Ultrason. Ferroelectr. Freq. Control* **2018**, *65*, 815–827. [CrossRef] [PubMed]
22. Kim, S.B.; Park, H. Comparison of MEMS PZT cantilevers based on d₃₁ and d₃₃ modes for vibration energy harvesting. *J. Microelectromech. Syst.* **2012**, *22*, 26–33. [CrossRef]
23. Park, J.C.; Park, J.Y. Modeling and characterization of piezoelectric d₃₃ mode MEMS energy harvester. *J. Microelectromech. Syst.* **2010**, *19*, 1215–1222. [CrossRef]
24. Truitt, A. Energy Harvesting through Wind Excitation of a Piezoelectric Flag-Like Harvester. Ph.D. Thesis, University of Alabama Libraries, Tuscaloosa, AL, USA, 2013. Available online: https://ir.ua.edu/bitstream/handle/123456789/1714/file_1.pdf?sequence=1&isAllowed=y (accessed on 1 September 2020).

25. Fang, H.B.; Liu, J.Q. Fabrication and performance of MEMS-based piezoelectric power generator for vibration energy harvesting. *Microelectron. J.* **2006**, *37*, 1280–1284. [[CrossRef](#)]
26. Erturk, A.; Inman, D.J. 1.4 Summary of the Theory of Linear Piezoelectricity. In *Piezoelectric Energy Harvesting*, 1st ed.; John Wiley & Sons: Hoboken, NJ, USA, 2011; pp. 9–12.
27. De Almeida, B.V.; Pavanello, R. Topology Optimization of the Thickness Profile of Bimorph Piezoelectric Energy Harvesting Devices. *J. Appl. Comput. Mech.* **2019**, *5*, 113–127.
28. Chopra, I. Review of state of art of smart structures and integrated systems. *AIAA J.* **2002**, *40*, 2145–2187. [[CrossRef](#)]
29. Maghsoudi Nia, E.; Wan Abdullah Zawawi, N.A.; Mahinder Singh, B.S. Design of a pavement using piezoelectric materials. *Mater. Werkst.* **2019**, *50*, 320–328. [[CrossRef](#)]
30. Viet, N.V.; Xie, X.D. Energy harvesting from ocean waves by a floating energy harvester. *Energy* **2016**, *112*, 1219–1226. [[CrossRef](#)]
31. Li, R.; Yu, Y. Harvesting energy from pavement based on piezoelectric effects: Fabrication and electric properties of piezoelectric vibrator. *J. Renew. Sustain. Energy* **2018**, *10*. [[CrossRef](#)]
32. Mishra, S.; Unnikrishnan, L.; Nayak, S.K.; Mohanty, S. Advances in Piezoelectric Polymer Composites for Energy Harvesting Applications: A Systematic Review. *Macromol. Mater. Eng.* **2018**, *304*, 1800463. [[CrossRef](#)]
33. Erturk, A.; Inman, D.J. 10.1.1 Effective Parameters of Various Soft Ceramics and Single Crystals. In *Piezoelectric Energy Harvesting*, 1st ed.; John Wiley & Sons: Hoboken, NJ, USA, 2011; pp. 301–3022.